Estimating Climatic Temperature Change in the Ocean with Synthetic Acoustic Apertures

Anatoly L. Fabrikant, John L. Spiesberger, Anisim A. Silivra, and Harley E. Hurlburt

Abstract—An acoustic tomography simulation is carried out in the eastern North Pacific ocean to assess whether climate trends are better detected and mapped with mobile or fixed receivers. In both cases, acoustic signals from two stationary sources are transmitted to ten receivers. Natural variability of the sound-speed field is simulated with the Naval Research Laboratory (NRL) layered-ocean model. A sequential Kalman–Bucy filter is used to estimate the sound speed field, where the *a priori* error covariance matrix of the parameters is estimated from the NRL model. A spatially homogeneous climate trend is added to the NRL fluctuations of sound speed, but the trend is not parameterized in the Kalman filter. Acoustic travel times are computed between the sources and receivers by combining sound speeds from the NRL model with those from the unparameterized climate trend. The effects of the unparameterized climate trend are projected onto parameters which eventually drift beyond acceptable limits. At that time, the unparameterized trend is detected. Mobile and fixed receivers detect the trend at about the same time. At detection time, however, maps from fixed receivers are less accurate because some of the unparameterized climate trend is projected onto the spatially varying harmonics of the sound-speed field. With mobile receivers, the synthetic apertures suppress the projection onto these harmonics. Instead, the unparameterized trend is correctly projected onto the spatially homogeneous portion of the parameterized sound-speed field.

Index Terms—Acoustic tomography, climate change, Kalman filtering, synthetic aperture imaging.

I. INTRODUCTION

THE IDEA of monitoring climatic temperature changes in the ocean with sound has attracted attention during the last decade [1]–[8]. The large scales in the ocean include a variety of processes such as persistent but time varying currents and gyres, Rossby waves, sporadic events like El Niño/Southern oscillation (ENSO), etc. These oceanic variations with different time and space scales may mask other trends in climate. It is topical to develop effective tools and algorithms to detect monotonic changes in temperature. The goal of this paper is to investigate the possibility that mobile receivers have advantages over fixed receivers in detecting and mapping monotonic trends in temperature with tomographic techniques. Simulations in this paper suggest that mobile receivers do have advantages over fixed receivers. This paper does not prove that mobile receivers are better than fixed receivers for detecting and mapping climatic changes. Future investigations, including those with data, will be necessary to more accurately assess the virtues of both approaches.

Fixed instruments have certain advantages in detecting climate change. Conceptually, all changes in acoustic travel times are due to changes in the ocean. This is not the case for mobile instruments, when travel times are changed both by the ocean and the variable geometry.

Another advantage of the fixed geometry is that time-independent biases can be removed from the data. The biases are eliminated by subtracting the first from subsequent travel times. This subtraction also removes the effects of small errors in the positions of the sources and the receivers. This simple subtraction cannot be applied to instruments that drift because the sections change with time and the biases depend on the geometry.

On the other hand, the use of mobile instruments is appealing because a synthetic aperture may enhance the accuracy and resolution of tomographic maps [9], [10]. There is no problem in accurately relocating failed instruments, as no attempt is made to occupy identical locations.

The simulation uses the Naval Research Laboratory's (NRL) layered-ocean model [11], [12] which has been used twice before to simulate tomography systems [13], [14]. It is the only eddy-resolving basin-scale model published to date that has been able to reproduce many features of the ocean's circulation associated with ENSO on time scales up to at least a decade [15]–[17]. We proceed from a potentially practical scheme for mapping climate change in the ocean with sound, proposed by Spiesberger *et al.* [13], [14]. The approach is based on the use of simulated data from drifting receivers. To simulate the change in climate, a spatially-uniform trend is added to the sound speed field computed from the NRL model.

II. SIMULATION OF SOUND-SPEED FIELD

The simulation is based on a precomputed sound speed field in a rectangular area within 192.5–239.5°E and 20.5–51.5°N. The sound speed is assumed to have the form

$$c(x, y, z, t) = c_0(x, y, z) + \delta c_{\mathrm{NRL}}(x, y, z, t) + \delta c_{\mathrm{ALG}} + \delta c_{\mathrm{TREND}}(t) \tag{1}$$

where $c_0(x, y, z)$ is the reference sound speed, obtained using Del Grosso's algorithm for sound speed [18] applied to temperatures and salinities from Levitus's climatological data [19]. The sound speed perturbation from the NRL model is δc_{NRL} and δc_{ALG} is the error in Del Grosso's sound-speed algorithm. The spatially homogeneous climate trend is denoted by $\delta c_{\mathrm{TREND}}$.

A. Parameterized Sound-Speed Fluctuations

The region for the simulation is a subdomain of the NRL model whose entire domain covers the Pacific within 20°S–62°N [15], [16]. The model has six constant-density layers, realistic bottom topography, and a horizontal grid resolution of 1/8°. It is forced by ECMWF winds from 1981–1995 [15]. It represents many features of the ocean including a Rossby wave that is linked to the 1982–1983 El Niño which traveled from California to Japan over a decade [17]. Modeled Rossby waves, linked to ENSO, set an important acoustic scale because they dominate modeled travel time changes in the eastern North Pacific [20].

Sound speed fluctuations, δc_{NRL}, are computed by assuming that vertical displacements of the model's density layers lead to adiabatic changes in the speed of sound [20]. The first twelve years are constructed from the first twelve years, 1981–1992, in which the NRL model was run. To simulate the next twelve years from 1993 to 2004, the same sound-speed field is used but with the time steps taken in reverse order. This extension guarantees that the sound speed field is continuous with time. Continuity of the sound-speed field is assured for the final twelve-year period, 2005–2016, by taking the sound speed to be the same as the first twelve years.

The sound-speed field from the NRL model is parameterized using a two-dimensional Fourier transform. The error of Del Grosso's sound-speed algorithm is modeled with the parameter δc_{ALG}. The details of how these are parameterized are given in [13].

B. Unparameterized Climate Trend

A climate trend, $\delta c_{\mathrm{TREND}}(t)$, is added to the "natural" variability, δc_{NRL}. The spatial structure of $\delta c_{\mathrm{TREND}}$ is assumed to be spatially homogeneous with a slow temporal evolution given by

$$\delta c_{\mathrm{TREND}}(t) = \mu_c \cdot \tau_c \cdot \left[\exp\left(\frac{t}{\tau_c} \right) - 1 \right] \qquad (2)$$

where τ_c is the time scale and μ_c is the temporal rate of change. We choose $\tau_c = 50$ years, a rough estimation of hypothetical global-warming trends from some general-circulation models [21]–[23]. The rate of change, μ_c, may be estimated from observations of the global average of the sea-surface temperature, which has been growing at about $\delta\theta \approx 7\cdot10^{-3}$ degrees per year for the last several decades.[1] The corresponding rate of sound speed change is therefore [18],

$$\mu_c \approx 4.5 \cdot \delta\theta = 3.3 \cdot 10^{-2} \ \mathrm{m} \cdot \mathrm{s}^{-1} \cdot \mathrm{yr}^{-1}, \qquad (3)$$

[1] NWS, Fifth Annual Climate Assessment 1993. Report of U.S. Department of Commerce, NOAA, National Weather Service, National Meteorological Center, Climate Analysis Center, Camp Spring, MD, p. 111, 1994.
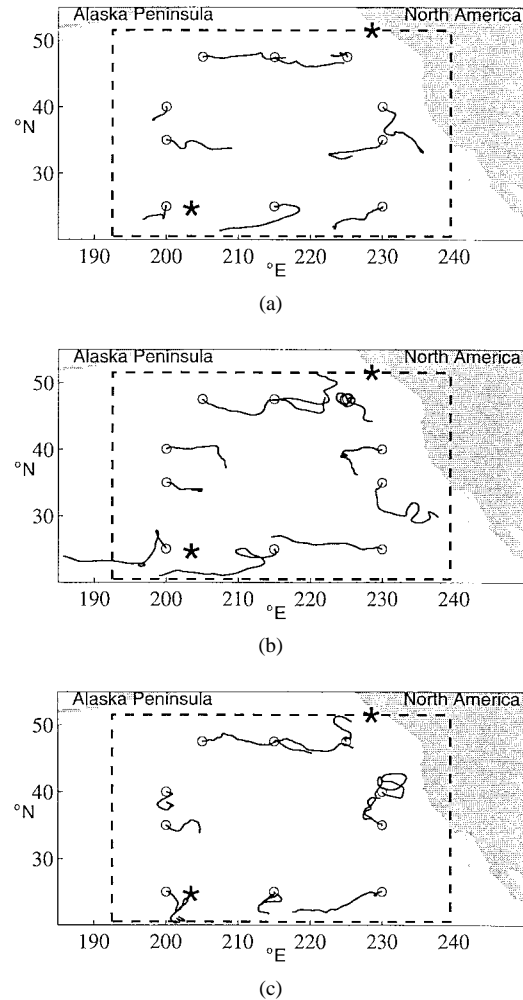

Fig. 1. Trajectories of drifting acoustic receivers for: (a) 1981, (b) 1985, and (c) 1992. Circles locate initial positions of the receivers and stars show positions of the acoustic sources.

The likely parameters onto which this trend will be projected are those representing the long-wavelength harmonics and the correction to the sound-speed algorithm.

III. SIMULATION OF ACOUSTIC DATA

The tomography simulation includes two transmitters and ten receivers (Fig. 1). A simulation of the 36-year period is made both for fixed and drifting receivers. Drifting receivers are deployed anew in the same initial positions at the first time step of each year. Each receiver drifts along a different path during each of the first twelve years because each is forced by the modeled currents which are different each year (Fig. 1). The trajectories have a periodicity of twelve years until the end of the 36-year simulation. The locations of the fixed receivers are the initial positions of the drifting receivers.

We assume that sound pulses propagate along geodesics. These sections are shown in Fig. 2(a) and (b) for the initial and the last time steps of 1985. For each geodesic, the acoustic travel time is computed the same way as in [13]. Simulated travel times are used for computation of the tomographic inverse.
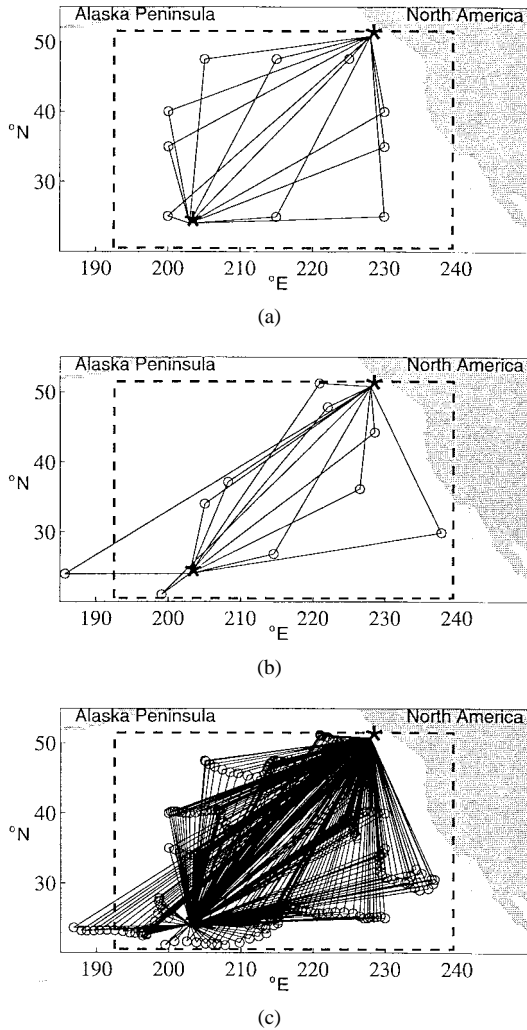
(a)

(b)

(c)

Fig. 2.   Tomographic sections for drifting acoustical receivers (a) at January 17, 1985, (b) at the end of 1985, and (c) accumulated for the year 1985.

(a)

(b)

(c)

Fig. 3.   (a) Sound-speed field computed from the NRL ocean model for January 17, 1985, in $\mathrm{m \cdot s^{-1}}$. (b) Tomographic reconstruction of the sound-speed field in $\mathrm{m \cdot s^{-1}}$, using two autonomously moored sources and ten drifting receivers. (c) Fraction of sound-speed variance at $4°$ resolution explained with tomography.

IV. PARAMETER VALUES FOR THE KALMAN FILTER

Details of the sequential Kalman–Bucy algorithm are described in [13]. Between time steps, the parameters are transitioned using a simple damped-persistence scheme. Variances and time scales for the parameters are the same as in cases 2 and 13 in [13], except as described below.

Biases in travel time due to eddies and internal waves are estimated following [13, eqs. (8), (9)]. The data are debiased by subtracting these estimates from the data. The errors in the bias estimates are accounted for by increasing the standard deviation of the noise components of the travel times in the Kalman filter. The standard deviations due to eddy and internal-wave corrections are

$$\sigma_{\mathrm{BIAS1}}[k] = 5 \times 10^{-6} R[k] \, (\mathrm{s}) \qquad (4)$$

and

$$\sigma_{\mathrm{BIAS2}}[k] = 3.4 \times 10^{-9} R^2[k] \, (\mathrm{s}) \qquad (5)$$

respectively, where the distance, in kilometers, between the source and the receiver is $R[k]$ at time step k of the simulation. These standard deviations are larger than assumed in [13].
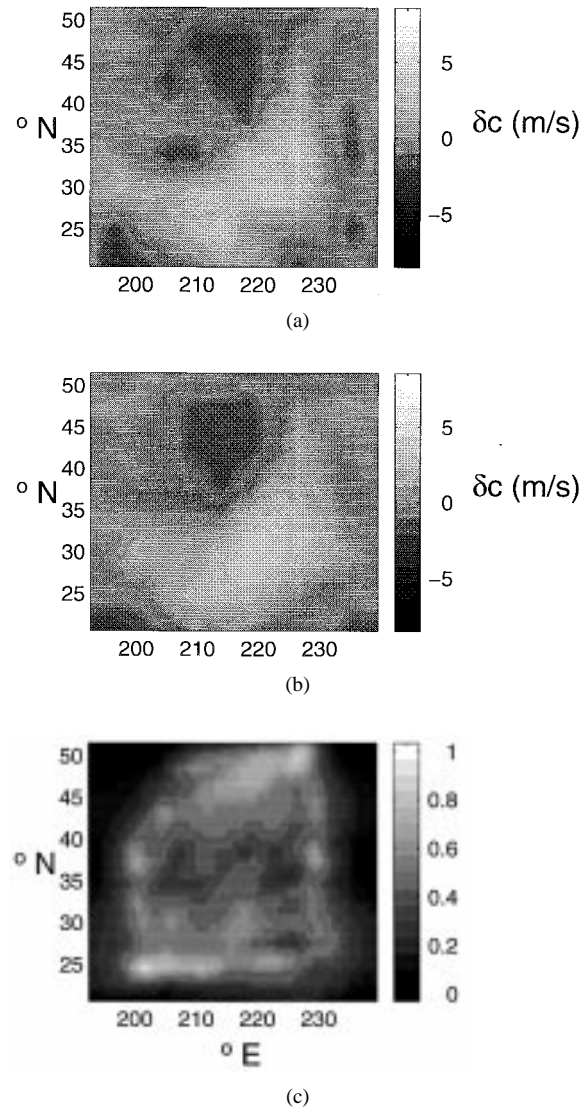
For fixed receivers, the standard deviations for the bias corrections are set to zero, as biases drop out of the problem (Introduction). The parameters for the error in the sound-speed algorithm and the corrections for the locations of the sources and receivers are also set to zero.

The modeled variances in travel times depend on horizontal wavenumber as $k^{-5.5}$ ([13, Fig. 12]). Consequently, modeled wavelengths exceeding 500 km dominate the contributions to modeled travel times. The correlation times of these harmonics are about a year ([13, Fig. 7]). During a year, the drifting receivers move significantly (Fig. 2), making it conceivable that the synthetic apertures could improve the tomographic maps.

The tomographic inverse is computed at 15.25-day intervals. We checked if the data fit the model, using the criterion described in [13, Appendix B]. For all the simulations, the data are found to fit the model.

DRIFTING

FUNDAMENTAL HARMONIC

FIXED

FUNDAMENTAL HARMONIC

FIRST LONGITUDINAL HARMONIC

FIRST LONGITUDINAL HARMONIC

SECOND LONGITUDINAL HARMONIC

SECOND LONGITUDINAL HARMONIC
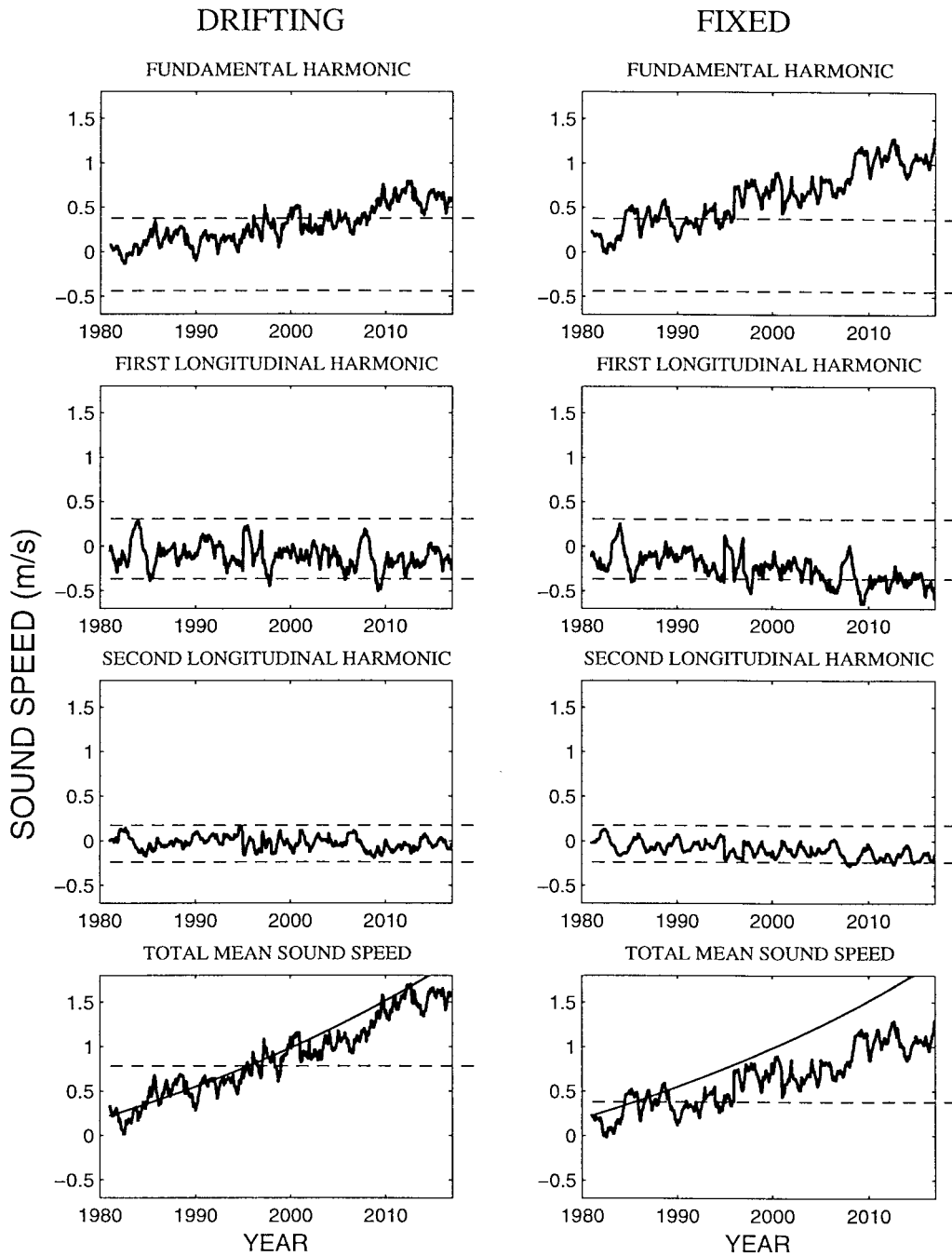
TOTAL MEAN SOUND SPEED

TOTAL MEAN SOUND SPEED

Fig. 4. Estimation of the climate with simulated acoustic tomography. Estimated values are shown by the dark solid line. *A priori* intervals of natural variability are shown by the dashed lines (two standard deviations). Light solid lines on the bottom panels show the unparameterized change in climate.

V. DETECTING UNPARAMETERIZED TRENDS

Using the Kalman filter, a sound-speed field is compared with the "true answer" provided by the NRL model (Fig. 3). As we consider relatively sparse tomographic sections, only large-scale features, including Rossby waves generated by the 1982–1983 El Niño, are accurately mapped. The quality of the tomographic reconstruction is measured with the fraction of sound-speed variance explained with tomography

$$P = 1 - \frac{V(x, y, t)}{V_a(x, y)} \quad (6)$$

where $V(x, y, t)$ is the variance of the sound-speed perturbations, averaged over $4° \times 4°$ regions, and $V_a(x, y)$ is the *a priori* variance of that average. The spatial distribution of P is shown in Fig. 3. The average and standard deviation of P taken over all squares, except those on the perimeter and on the second from the most right column, is 0.81 ± 0.06, independent of whether the instruments are fixed or drifting. The excluded regions are those in which few tomographic sections reside.

Fig. 4 shows the parameters for the fundamental and first two longitudinal harmonics from the Kalman filter using drifting and fixed receivers. The bottom row shows the total-mean

sound-speed field. For drifting receivers, the total mean is the sum of the fundamental harmonic and the estimated correction of the sound-speed algorithm, δc_{ALG}. For fixed receivers, where the error of the sound-speed algorithm drops out of the problem, the total-mean sound speed is the fundamental harmonic.

The *a priori* limits for the total mean speed of sound are defined as two standard deviations of the *a priori* parameters. The limit for drifting receivers is about twice that for fixed receivers (bottom panels, Fig. 4). This occurs because there is an additional model parameter and corresponding additional uncertainty for drifting receivers due to the fact that the drifting receiver case includes a correction for errors in the sound-speed algorithm.

The limit for the total mean speed of sound for drifting receivers is independent of the accuracy with which these receivers are navigated, i.e., 10 m. A previous simulation has demonstrated that the errors of the tomographic reconstruction (Fig. 3) are not very sensitive to the magnitude of navigational errors [13].

Some parameters in Fig. 4 have trends which go beyond their *a priori* limits. For both drifting and fixed receivers, the trends are inconsistent with *a priori* limits after 1.5–2 decades, at which time the trends do not cross below these limits. The inconsistency arises because of the unparameterized change in climate that is added to the sound-speed field in the NRL model (1).

For drifting receivers, this climate change is projected onto the fundamental harmonic and the parameter for the correction to the sound-speed algorithm, δc_{ALG}. The total spatially homogeneous component of the sound-speed field reproduces the unparameterized climate change fairly well (lower left panel, Fig. 4).

For fixed receivers, the spatially homogeneous components of the parameterized sound-speed field do not accurately follow the correct climate trend. Instead, part of the unparameterized change in climate is projected onto low-order harmonics of the field (Fig. 4). The reason for the reconstruction error is based on the fact that tomography only contains information about the horizontal wavenumbers which are aligned with the sections [24]. The number and variety of sections is insufficient to suppress the mapping of the climate trend onto low-order harmonics of the spatial field.

With drifting receivers, the synthetic apertures yield a much richer sampling of horizontal-wavenumber space during a correlation time interval of the model [Fig. 2(c)]. This better suppresses the projection of the unparameterized climate trend onto low-order harmonics. Consequently, the unparameterized change in climate is primarily projected onto the spatially homogeneous parameters of the Kalman filter.

In order to test whether the result in the left column of Fig. 4 is sensitive to the trajectories of drifting receivers, a simulation is made where each receiver repeats the trajectory it has during 1985 during each of 36 years. The new graph for the spatially homogeneous component of the field is then different from the one shown in the left column of Fig. 4, but the difference is less than two standard deviations. So this difference is statistically insignificant.

VI. Discussion

The simulations show that acoustic tomography is useful for mapping unparameterized climate variability. The unparameterized change shows up in parameters of the Kalman filter. In a certain time, which depends on the number of data, some of these parameters go beyond reasonable limits. Then, we can recognize that some unparameterized trend is occurring. For both fixed and drifting receivers, the trends for the total mean sound speed cross, and do not come back below, the limits of two standard deviations in 1.5–2 decades (bottom panels, Fig. 4).

These results are not meant to suggest that a climate change due to human activity can be detected in one or two decades with acoustic tomography, although other researchers have argued that this is possible [2], [3], [6]. To detect climate change due to human activity, we believe it is necessary to better quantify the natural variability of the climate system [20].

Although the *a priori* variance of the total-mean sound-speed field is higher for drifting receivers (dashed line, bottom row, Fig. 4) both fixed and drifting instruments are capable of detecting the unparameterized trend at about the same time. Consequently, it may be unnecessary to use fixed sources and receivers that are cabled to shore. Assimilation of data from different sections throughout time ought to drastically reduce the cost of observing climate change [9].

There are, however, differences in the performance of drifting and fixed instruments. Fixed receivers do not pick up the correct value of the unparameterized change in climate at the correct spatial scale. By virtue of their synthetic aperture, mobile receivers more accurately map the unparameterized changes onto the correct scales in space.

References

[1] J. L. Spiesberger, T. G. Birdsall, and K. Metzger, "Acoustic thermometer," ONR Contract N00014-82-C-0019, available through the Woods Hole Oceanographic Institution, Woods Hole, MA 02543, 1983.
[2] W. Munk and A. M. G. Forbes, "Global ocean warming: An acoustic measure?," *J. Phys. Oceanogr.*, vol. 19, pp. 1765–1778, 1989.
[3] A. J. Semtner and R. M. Chervin, "Environmental effects on acoustic measures of global ocean warming," *J. Geophys. Res.*, vol. 95, pp. 12 973–12 982, 1990.
[4] J. L. Spiesberger and K. Metzger, "Basin-scale tomography—A new tool for studying weather and climate," *J. Geophys. Res.*, vol. 96, pp. 4869–4889, 1991.
[5] ———, "Basin-scale monitoring with acoustic thermometers," *Oceanography*, vol. 5, pp. 92–98, 1992.
[6] U. E. Mikolajewicz, E. Maierreimer, and T. P. Barnett, "Acoustic detection of greenhouse-induced climate changes in the presence of slow fluctuations of the thermohaline circulation," *J. Phys. Oceanogr.*, vol. 23, pp. 1099–1109, 1993.
[7] J. L. Spiesberger, D. E. Frye, J. O'Brien, H. E. Hurlburt, J. W. McCaffrey, M. Johnson, and J. Kenny, "Global acoustic mapping of ocean temperatures (GAMOT)," in *IEEE Oceans'93 Proc.*, 1993, paper I-253.

[8] W. Munk, P. Worcester, and C. Wunsch, *Ocean Acoustic Tomography.* Cambridge, U.K.: Cambridge, 1995, p. 450.

[9] J. L. Spiesberger, "Is it cheaper to map Rossby waves in the global ocean than in the global atmosphere?," *J. Marine Environ. Eng.*, vol. 1, pp. 83–90, 1993.

[10] J. L. Spiesberger, D. E. Frye, J. J. O'Brien, H. E. Hurlburt, J. McCaffrey, M. Johnson, M. Leach, and J. Kenny, "Global acoustic mapping of ocean temperatures (GAMOT)," in *Proc. Second Eur. Conf. Underwater Acoustics*, 1994, vol. II, pp. 1031–1036.

[11] H. E. Hurlburt and J. D. Thompson, "A numerical study of loop current intrusions and eddy shedding," *J. Phys. Oceanogr.*, vol. 10, pp. 1611–1651, 1980.

[12] A. J. Wallcraft "The Navy layered ocean model users guide," Nav. Res. Lab., Stennis Space Center, MI, NOARL Rep. 35, 1991.

[13] J. L. Spiesberger, A. L. Fabrikant, A. A. Silivra, and H. E. Hurlburt, "Mapping climatic temperature changes in the ocean with acoustic tomography: Navigational requirements," *IEEE J. Oceanic Eng.,* vol. 22, pp. 128–142, 1997.

[14] A. A. Silivra, J. L. Spiesberger, A. L. Fabrikant, and H. E. Hurlburt, "Acoustic tomography at basin scales and clock errors," *IEEE J. Oceanic Eng.* vol. 22, pp. 143–150, 1997.

[15] H. E. Hurlburt, A. J. Wallcraft, W. J. Schmitz, Jr., P. J. Hogan, and E. J. Metzger, "Dynamics of the Kuroshio/Oyashio current system using eddy-resolving models of the North Pacific Ocean," *J. Geophys. Res.*, vol. 101, no. C1, pp. 941–976, 1996.

[16] G. A. Jacobs, W. J. Teague, J. L. Mitchell, and H. E. Hurlburt, "An examination of the North Pacific Ocean in the spectral domain using GEOSAT altimeter data and a numerical ocean model," *J. Geophys. Res.*, vol. 101, no. C1, pp. 1025–1044, 1996.

[17] G. A. Jacobs, H. E. Hurlburt, J. C. Kindle, E. J. Metzger, J. L. Mitchell, and W. J. Teague, "Decade scale transpacific propagation and warming effects of an El Niño anomaly," *Nature*, vol. 370, pp. 360–363, 1994.

[18] V. A. Del Grosso, "New equation for the speed of sound in natural waters with comparison to other equations," *J. Acoust. Soc. Amer.*, vol. 56, pp. 1084–1091, 1974.

[19] S. Levitus, "Climatological atlas of the world ocean," NOAA Prof. Paper 13, U.S. Government Printing Office, Washington, DC, 1982.

[20] J. L. Spiesberger, H. E. Hurlburt, M. Johnson, M. Keller, S. Meyers, and J. O'Brien, "Acoustic thermometry data compared with two ocean models: The importance of Rossby waves and ENSO in modifying the ocean interior," *Dyn. Atmos. Oceans*, vol. 26, no. 4, 1998.

[21] T. M. L. Wigley and S. C. B. Raper, "Implications for climate and sea level of revised IPCC emission scenarios," *Nature,* vol. 357, pp. 293–300, 1992.

[22] J. Hansen, A. Lacis, R. Ruedy, M. Sato, and H. Wilson, "How sensitive is the world's climate?," *Natl. Geogr. Res. Exploration*, vol. 9, pp. 142–158, 1993.

[23] J. M. Murphy, "Transient response of the Hadley center coupled ocean-atmosphere model to increasing carbon dioxide. 3. Analysis of global-mean response using simple models," *J. Climate*, vol. 8, pp. 496–514, 1995.

[24] B. D. Cornuelle, W. H. Munk, and P. F. Worcester, "Ocean acoustic tomography from ships," *J. Geophys. Res.*, vol. 94, no. C4, pp. 6232–6250, 1989.

John L. Spiesberger was born in Jackson, MI, on November 14, 1953. He received the A.B. degree in physics from the University of California at Berkeley in 1975 and the Ph.D. degree in oceanography from the University of California at San Diego in 1980.

From 1982 to 1992, he conducted research at Woods Hole Oceanographic Institution, Woods Hole, MA, and thereafter joined the Department of Meteorology at Pennsylvania State University, University Park, with a joint appointment at the Applied Research Laboratory. He has contributed to the fields of underwater acoustics, physical oceanography, inverse theory, signal processing, and bioacoustics.

Anisim A. Silivra was born in Slaviansk, Ukraine, on February 26, 1954. He received the Masters degree in general physics in 1976 and the Ph.D. degree in theoretical and mathematical physics in 1983, both from Kiev State University.

In 1983, he joined Kiev University, working on linear and nonlinear theory of interaction of electromagnetic waves with electron beams and plasmas. In 1994, he joined the Department of Meteorology of Pennsylvania State University (Penn State), State College. He contributed to underwater acoustic tomography simulation and development of inverse technique for undetermined systems. Since 1996, he has been with the Applied Research Laboratory at Penn State.

Harley E. Hurlbert received the B.S. degree from Florida State University in 1974 after serving as a Weather Officer in the U.S. Air Force from 1965 to 1969.

He did Post-Doctoral studies in the Advanced Studies Program at the National Center for Atmospheric Research in Boulder, CO, from 1974 to 1975. Since then, he has done ocean modeling for the U.S. Navy, first as a contractor at JAYCOR for the Naval Research Laboratory, Washington, DC, then from 1977 for the Naval Ocean Research and Development Activity, which later became the Naval Oceanographic and Atmospheric Research Laboratory, and which merged with the Naval Research Laboratory in 1992, all in a location at Stennis Space Center, MS. In addition, he is an Adjunct Faculty Member at Florida State University and the University of Southern Mississippi. His primary research interests are ocean modeling and prediction, especially the investigation of ocean dynamics using eddy-resolving global and basin-scale ocean models.

Anatoly L. Fabrikant received the M.S. degree in physics from the State University of Gorky, Russia, in 1973, and the Ph.D. degree in nonlinear dynamics from the Institute of Applied Physics, Russian Academy of Science, Nizhny Novgorod, Russia, in 1991.

He worked for 20 years in the Institute of Applied Physics, Russian Academy of Sciences. He then worked at Jet Propulsion Laboratory, NASA, and then became a Senior Research Associate in the Department of Meteorology, Pennsylvania State University, University Park. He is now with Therma-Wave, Inc., Fremont, CA. His research interests are in fluid dynamics, oceanography, wave theory, acoustics, nonlinear dynamics, and remote sensing.

Dr. Fabrikant is a member of the Acoustical Society of America and the American Geophysical Union.